

Article

# Effect of Additional Shielding Gas on Welding Seam Formation during Twin Wire DP-MIG High-Speed Welding

Yu Hu, Jiayang Xue \*, Changwen Dong, Li Jin and Zhanhui Zhang 

School of Mechanical and Automotive Engineering, South China University of Technology, Guangzhou 510641, China; scshuyu@163.com (Y.H.); d.changwen@mail.scut.edu.cn (C.D.); jinli8756@163.com (L.J.); 201610100399@mail.scut.edu.cn (Z.Z.)

\* Correspondence: mejiaxue@scut.edu.cn; Tel.: +86-020-2223-6360

Received: 4 August 2018; Accepted: 10 September 2018; Published: 14 September 2018



**Abstract:** For diminishing welding defects such as incomplete penetration, which may easily occur during the twin wire Double Pulsed Metal Inert Gas (DP-MIG) high-speed welding, a novel method using additional shielding gas is introduced in this paper. A branch for the additional shielding gas was specially set near the back end of the protection hood for the DP-MIG nozzle. The constructed gas branch was used for enabling manual intervention in the formation of a high-temperature solid–liquid weld seam just emerging from the nozzle and also for secondary gas protection on the surface of the weld seam. The butt welding test was carried out in the 2205 duplex stainless steel plate and the weld seam was then characterized by a tensile test, metallographic analysis, X-ray non-destructive testing (NDT), hardness analysis, and impact test. The results showed that the introduction of an appropriate amount of additional shielding gas can effectively improve and diminish the unfused weld seam and also improve the mechanical properties such as the tensile properties of the weld joint, the hardness and toughness of the weld joints. Therefore, the introduction of additional shielding gas has further research potential in theory and process practice.

**Keywords:** additional shielding gas; twin wire; DP-MIG; high-speed welding; welding seam formation

## 1. Introduction

With the developments in marine engineering, aeronautics and aerospace, transportation and other industries, welding technology has undergone continuous development. Improving the efficiency of welding production, achieving welding automation, and improving welding quality have become key issues in the development of welding technology [1]. Twin wire Double Pulsed Metal Inert Gas (GMAW) welding technology can perform high-speed welding and achieve a high deposition rate and is therefore considered a promising topic for research internationally [2–4] with many researchers being actively involved in related studies.

Ueyama et al. studied the effects of the inclination angle between the leading and trailing wire, the twin wire spacing and the welding current ratio on the formation of weld bead in the high-speed welding process. With the basic requirements of avoiding undercut and hump bead, the best set of parameters for high-speed welding was obtained with a welding speed up to 4.5 m/min [5]; Ueyama et al. investigated the effects of the distance between the leading and trailing wire and the mixing ratio of gas on the abnormal arc voltage and arc interruption in twin-wire GMAW welding. Additionally, the reasonable ranges for welding wire distance and gas mixing ratio were given [6]. Through pulse timing control and arc length control of the twin wire GMAW welding, Ueyama and other researchers succeeded in minimizing the arc intervention, avoiding arc interruption, establishing stable

control using arc length control and confirming that the stable control is not affected by the fluctuation in the feeding speed and length extension of the wire [7]. Considering the steel plate welding process applied in the shipbuilding industry, Sterjovski and other researchers investigated the formation mechanism of solidified cracks in twin wire GMAW welding and proposed a solution to diminish the crack generation [8]. Wu et al. studied the stability of three phase arcs: independent, alternating, and independent of twin wire DP-GMAW welding and its effects on weld quality and microstructure [9]. Gery et al. predicted the transient temperature distributions and temperature variations of the welded plates during welding [10]. Armentani et al. analyzed temperature distribution in butt weld joints, and successive thermo-mechanical analyses were performed to evaluate resulting residual stresses [11]. Hazvinloo et al. analyzed the effects of various FCAW welding parameters on weld width and tensile properties of weld metal extracted of butt joint [12]. Armentani et al. used a parametric model and the elements birth and death in single-pass butt welded joint to simulate the weld filler variation with time [13]. Somashekara et al. studied the effect of area-filling paths on the residual stresses developed during twin-wire arc weld-deposition [14]. Hang et al. studied the bypass coupling technique which was employed in twin-wire indirect arc welding (TWIAW) to improve its penetration [15]. Wen et al. investigated microstructural evolution and mechanical properties of an ultra-high strength structural steel welded joint at different heat inputs in the metal active gas arc (MAG) welding technique [16]. Ruan et al. studied the microstructures, penetration and mechanism of the welding joint by twin wire Metal Inert Gas (MIG) welding with  $\text{Cr}_2\text{O}_3$  activating flux [17]. Cai et al. investigated a three-component shielding gas mixture used in tandem with narrow gap pulsed GMAW, and the effect of its composition on arc behaviors and weld formation [18]. Reis et al. investigated the effects of arc length, torch angle, and high-frequency current pulsing on the arc resistance to extinction in tandem GMAW [19]. The researchers showed results that an increase in the welding speed brings to the fore some issues that are different from those in conventional welding. For instance, incomplete penetration, hump bead, bead discontinuity, and gas pore formation are the main defects that occur in the twin wire GMAW welding [20–22].

Based on the twin wire pulsed MIG welding, a new method that involves introducing additional shielding gas is proposed, which can extend the gas protection time for the weld seam and manually intervene in the formation of the weld seam. Making use of the mechanical properties and air-shielding characteristics of the gas jet, the two functions of shielding gas: manual intervention in the formation of the weld seam and protection of the weld seam, can be achieved simultaneously. By studying the effects of twin wire DP-MIG on weld formation, microstructure, and mechanical properties under the supply of additional shielding gas, the welding defects in high-speed welding process like undercut and hump weld can be reduced, and low cost gas shielded twin wire welding for high speed welding can be performed.

## 2. Experimental Methods and Materials

### 2.1. Experimental Equipment and Methods

The schematic diagram of the twin wire double pulsed MIG welding with additional shielding gas is shown in Figure 1. The data acquisition platform for the welding test consists of a self-designed integrated digital welding power source, an additional device to supply shielding gas, a Panasonic wire feeder and a feeding device with water cooling box, an automatic screw travel control device, Advantech industrial computer, Advantech signal acquisition card, and arc dynamic wavelet analyzer that can acquire real-time signals such as current, voltage, energy input, and dynamic resistance. Compared with the conventional shielding gas device, the additional shielding gas device supplements a three-way adjustable valve, gas flow meters for branch B (branch for shielding gas entering into the welding torch) and branch C (branch for supplementing shielding gas), an electric gas valve 2 and a one-way valve, and the gas nozzle for additional shielding gas is close to the nozzle of the welding torch. Integrated with the original welding equipment, the new device constitutes a new gas path

system with an adjustable gas flow in every branch and the readable flow rate. The new gas flow system works on the following principle: the gas source of the cylinder passes through the gas conduit into the electric gas valve 1 in the gas supply branch. Herein, the electric gas valve is controlled by the button at the torch handle. When the welding starts, the gas valve is opened and the shielding gas enters the gas conduit in the wire feeder through the valve. The gas circuit passes through the wire feeder and is connected to the A end of the three-way adjustable valve. With a knob, the three-way gas adjustable valve can realize the amount distribution of the gas coming from the main branch, and the B and C outputs allow appropriate amounts of gas through outlet pipes. The gas flow in C branch is the newly-added supplementing shielding gas flow. The gas flow outputs from the three-way valve port C. The on/off state is controlled by the electric gas valve 2, and the gas flow passes through the one-way valve, following which it is ejected from the nozzle for the additional gas. The gas flow ejected by the nozzle covers the weld seam excluding just the arc zone and provides a stable, continuous gas protection to the weld seam that would otherwise be exposed to air.

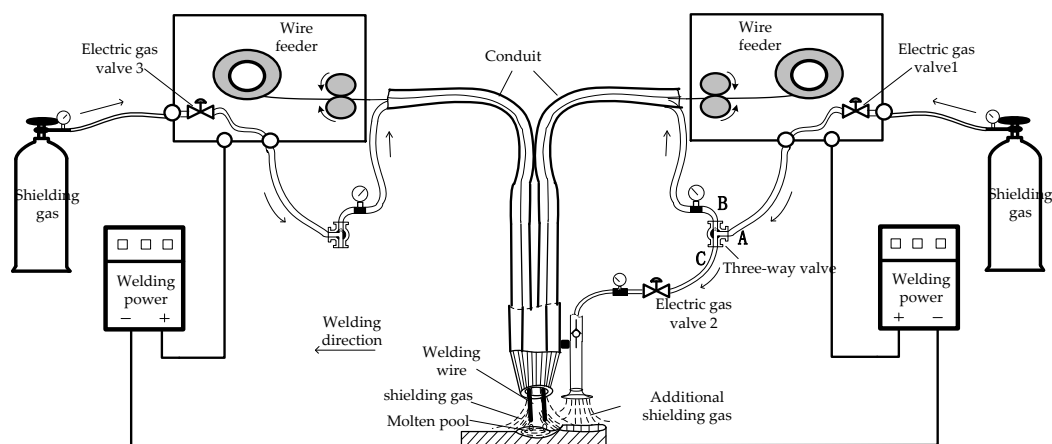


Figure 1. Schematic diagram of the twin wire pulsed MIG welding under additional shielding gas.

### 2.2. Experimental Materials and Processing

The base metal is a 2205 duplex stainless steel plate, with dimensions of 250 × 100 × 3 mm. ER2009 weld wire with a diameter of 1.2 mm is adopted. Their chemical compositions are shown in Table 1. The peak and base current of the leading and trailing wire are 350 A and 120 A. The weld frequency is 3 Hz, and the other weld parameters such as the flow rate of additional shielding gas, and weld speed are shown in Table 2.

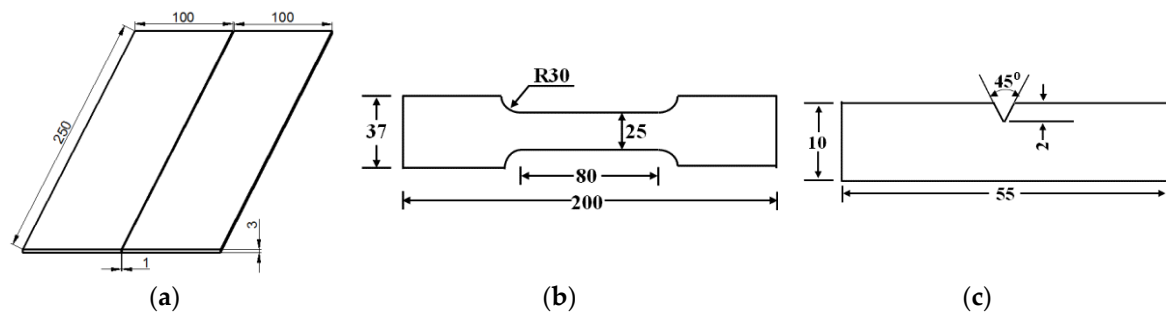
Table 1. Chemical compositions of 2205 and ER2209.

Materials	C	Mn	Si	Cr	Ni	Mo	N	S	P
2205	0.024	≤2.0	≤1.0	22–23	4.5–6.5	3.0–3.5	0.15–0.2	≤0.02	≤0.03
ER2209	0.025	1.6	0.3	22.5	9.5	3.1	0.16	0.01	0.025

Table 2. Main processing parameters of weld process.

Sample Number	Flowrate of Additional Shielding Gas L/min	Weld Speed cm/min
1	0	160
2	12	160
3	0	180
4	12	180
5	0	200
6	12	200

In this paper, flat butt welding is used, and the gap between two plates is 1 mm. The draft of plate and all dimensions are shown in Figure 2a. The additional shielding gas is argon (Ar) with a purity of 99.99% and a flow rate of 12 L/min. Before the welding test, the surface of the sample is first grounded with sandpaper to remove the oxide deposits, and the surface of the sample is wiped clean with alcohol. The welding starts after the surface is dried. The self-developed wavelet analyzer is used to acquire voltage and current signals during the welding process. The waveforms of current and voltage are statistically analyzed. After welding, a spark discharge wire cutter is used to remove 20 mm from both ends of the weld, and samples for the tensile test, metallographic, and impact samples are cut from the weld as vertical sections. The dimensions of the test samples are shown in Figure 2b,c. The metallographic test specimens are prepared using standard metallographic procedures. The microstructure of the welded joint is observed and analyzed using an Olympus optical microscope (OM) (Olympus, Shibuya, Japan) and scanning electron microscopy (SEM) (Hitachi, Tokyo, Japan). The Rockwell hardness test is performed on the polished and etched specimens by the Rockwell hardness test machine (Buehler, Lake Bluff, IL, USA). For each test point, the test time is 15 s, with a load of 150 kg and a step size of 1 mm. The tensile test is conducted on the test machine (INSTRON, Boston, MA, USA) at room temperature. Tensile test specimens are produced following ASTM E8 at the crosshead speed 3 mm/min, and 3 specimens are tested for each welded joint. In order to evaluate the impact toughness of the welded joint, the Charpy impact test (with a test specimen thickness of 3 mm) is carried out, and the Charpy impact test samples are prepared in accordance with ISO 5173:2000. After the tensile test and the impact test, the fracture morphology of the welded joint is observed by SEM.



**Figure 2.** Dimensions of test specimens (unit: mm): (a) Draft of plate and all dimensions, (b) Specimen for tensile test, (c) Specimen for Charpy impact test.

### 3. Results


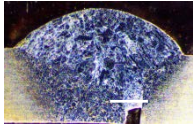

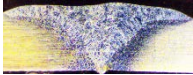
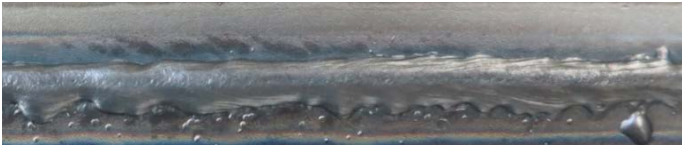
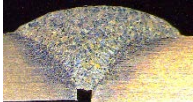

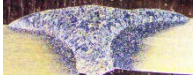

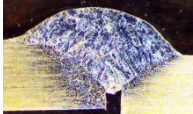

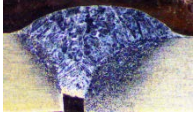
#### 3.1. Formation of the Weld Seam

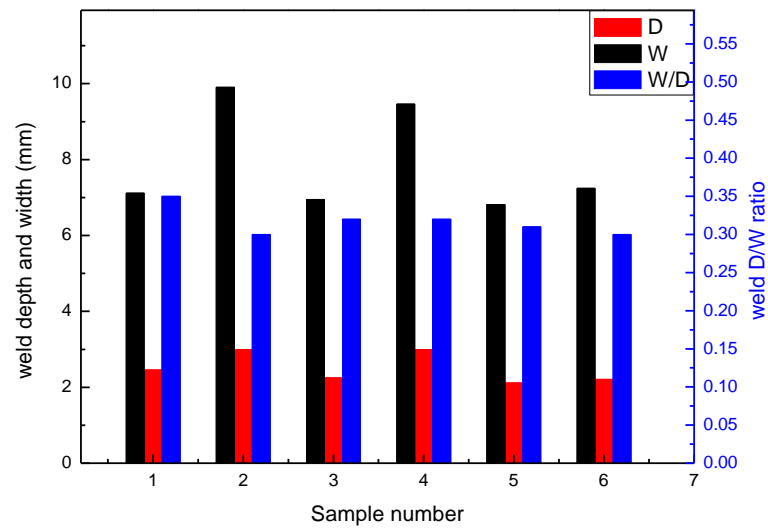
It can be seen from Table 3 that at the same weld speed and weld current, the weld seam obtained with additional shielding gas has larger width and deeper penetration. With the increase in welding speed, both the penetration depth and weld width decrease. In this paper,  $D$  is weld depth,  $W$  is weld width,  $D/W$  is the ratio of weld depth and weld width. The lower  $D/W$  ratio than the weld formed without the additional shielding gas as shown in Figure 3a. It can be seen from Figure 3b,c that Sample 1 has obvious unfused defects and Sample 2 is completely penetrated. This comparison indicates that without changing the welding current and welding speed, adding only one branch for the additional shielding gas can effectively improve and diminish the unfused defects of the weld. The shape of the obtained welds varies greatly and the morphologies of welds formed with additional shielding gas are obviously superior to those without shielding gas. Similarly, Sample 3 has obvious unfused defects as shown in Figure 3d, and Sample 4 is completely penetrated in Figure 3e. In contrast to Figure 3b,d, the penetration depth and weld width decreases with the increase of welding speed. It can be seen from Figure 3f,g that Sample 6 has slightly larger width and deeper penetration than Sample 5, but both samples have unfused defects. As the welding speed increases, the heat transferred will



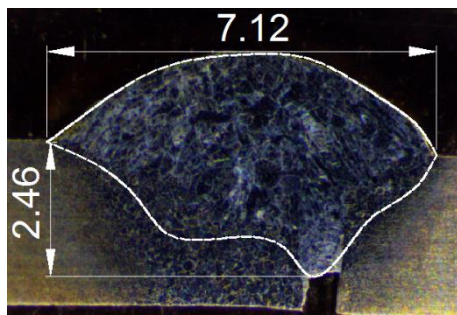
decrease synchronously, and the heat input will decrease significantly if the effective power remains unchanged. As shown in Figure 3g, when the welding speed increases to 2 m/min, the welding heat input decreases, resulting in narrow weld width and insufficient penetration. Although additional gas can improve part of the weld formation and stir pool, it cannot completely solve the problem of unfused defects caused by insufficient heat input. It can be concluded from Figure 3h that the part of the weld bead without additional shielding gas is unevenly curved formation, and the weld is narrow and the penetration depth is insufficient, indicating poor formation of the weld bead. After the additional shielding gas is introduced, the surface of the weld seam is relatively smooth and uniform. The weld surface exhibits an obvious fish scale-like weld bead, with larger width and deeper penetration. This is attributed to the two actions of the additional shielding gas: (1) the impact force generated by the gas flow can significantly change the original natural solidification mode of the weld pool metal, resulting in the improvement of the weld formation and stirring of the molten pool; (2) the gas flow hood formed during the gas impact can effectively extend the shielding time for the surface of the weld seam and feed the heat back to the molten pool directionally.

**Table 3.** The weld shape and section of joints.

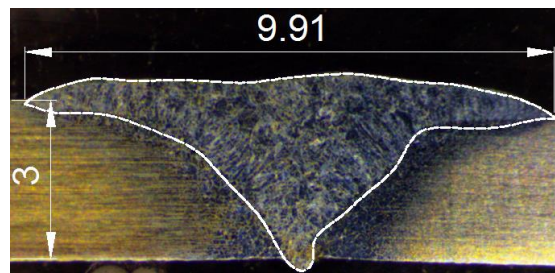
No.	Weld Shape	Section of Joints
1		
2		
3		
4		
5		
6		



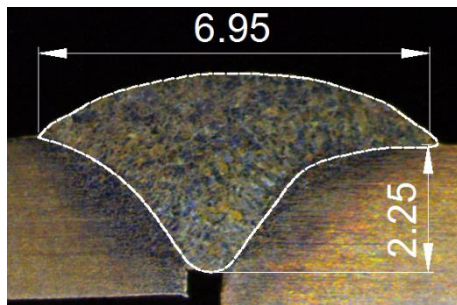
(a)



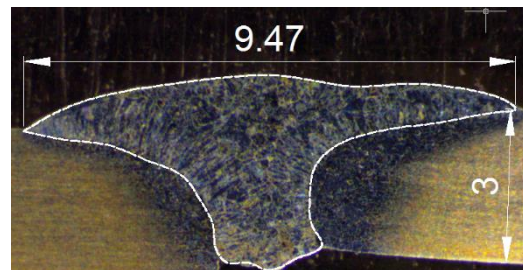
(b)



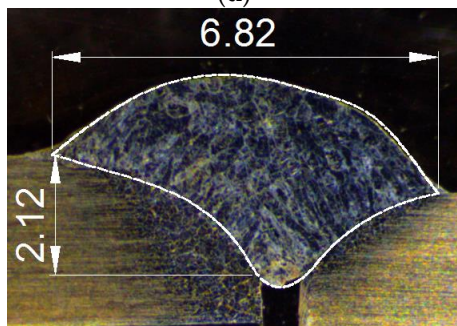
(c)



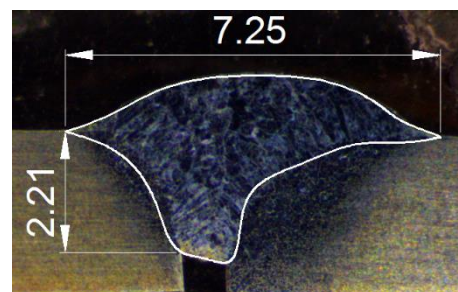
(d)



(e)

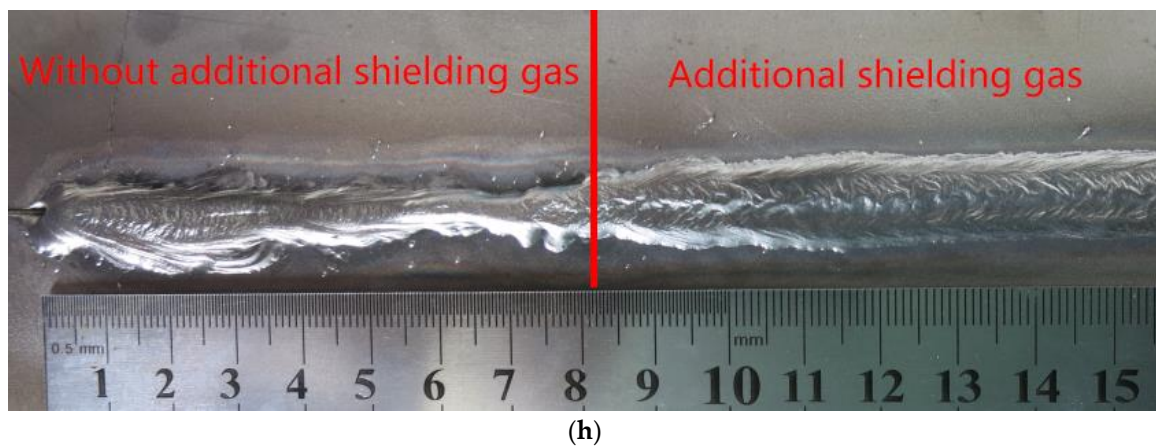


(f)



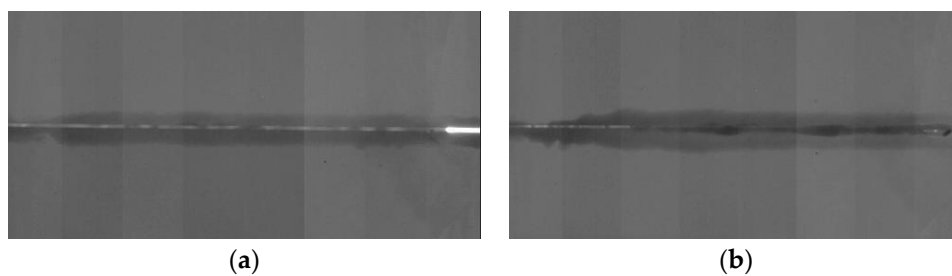
(g)

Figure 3. Cont.



**Figure 3.** Morphology of the weld seam: (a) Penetration depth and width/depth, (b) The cross-section of joint of Sample 1, (c) The cross-section of joint of Sample 2, (d) The cross-section of joint of Sample 3, (e) The cross-section of joint of Sample 4, (f) The cross-section of joint of Sample 5, (g) The cross-section of joint of Sample 6, (h) the comparison before and after the introduction of additional shielding gas.

After welding, X-ray NDTs are employed to examine the defects in the weld. As the weld shapes are similar when the samples are welded at 160, 180 and 200 cm/min, we only carry out X-ray NDT at the weld speed of 160 cm/min. The results of X-ray NDT testing of Sample 1 and Sample 2 are shown in Figure 4. When the welding speed is 1.6 m/min, no obvious gas pores are found in the weld seams with and without additional shielding gas, indicating that both welds have good compactness.



**Figure 4.** X-ray NDT photograph: (a) X-ray NDT for weld seam in Sample 1, (b) X-ray NDT for weld seam in Sample 2.

### 3.2. Results of Metallographic Tests

There are 6 samples selected to analyze the fusion zone, heat-affected zone, and base metal of the weld seam. The microstructure of the heat-affected zone is observed under a magnification of 50 times. The Figure 5a–f is corresponded to the Sample 1–6 respectively. The matrix is ferrite, while the strip and block structures are austenite. The microstructure of the heat-affected zone has irregular strip and block-like features, and the characteristics of two-phase are interpenetrated distribution. In Sample 1, a heat-affected zone of 200–1600  $\mu\text{m}$  width is shown in Figure 5a, while the heat-affected zone with 150–1000  $\mu\text{m}$  width of Sample 2 as shown in Figure 5b is narrower than that of the heat-affected zone in Sample 1. In Sample 3, a heat-affected zone of 200–1200  $\mu\text{m}$  width is shown in Figure 5c, while the heat-affected zone with 300–800  $\mu\text{m}$  width of Sample 4 as shown in Figure 5d is narrower than that of the heat-affected zone in Sample 3. In Sample 5, a heat-affected zone of 500–600  $\mu\text{m}$  width is shown in Figure 5e, while the heat-affected zone with 150–400  $\mu\text{m}$  width of Sample 6 as shown in Figure 5f is narrower than that of the heat-affected zone in Sample 5. This is because the fluidity of the molten pool metal in the presence of additional shielding gas is better than that without additional gas due to the action of external gas flow. The better fluidity provides more driving force for the diffusion of



the metal and a shorter residence time in the liquid state, and so the extent of its heat-affected zone is smaller than that of the weld seam without additional shielding gas.

The microstructure of the fusion zone is observed under a microscope at a magnification of 500 times. The fusion zone exhibits an as-cast dendritic crystal structure, which is mainly austenite. It can be seen that a large number of austenite segments precipitate with the feather and dendritic shapes distributed in the grain boundaries and crystals of ferrite and form a relatively obvious boundary with the base metal 2205 as shown in Figure 5g. The coarse and large Widmanstatten structure appears in the fusion area, indicating that the hardness and toughness of the metal become poorer while the brittleness of the weld pool metal increases. The grain size in the weld fusion zone in Sample 1 is obviously coarser and larger than that of the Sample 2, as shown in Figure 5g,h. The grain size in the weld fusion zone in Sample 3 is obviously coarser and larger than that of the Sample 4, as shown in Figure 5i,j. The grain size in the weld fusion zone in Sample 5 is obviously coarser and larger than that of the Sample 6, as shown in Figure 5k,l. This is because there is no additional shielding gas, the metal has poorer fluidity and the liquid metal has a longer residence time. As a result, the austenite in the fusion zone continues to increase, which increases the brittleness of the weld pool metal, thereby indicating that the hardness and toughness obtained in Sample 1 are less favorable.

The Rockwell hardness test results of Samples 1–6 are shown in Figure 6. It can be observed that the hardness of the heat affected zone (HAZ) metal is higher than that of base metal (BM) and weld metal (WM), and the hardness of weld metal is higher than that of base metal. The reason may be that the HAZ is the junction of BM and WM, the grain distribution is not uniform, and it is easy to form welding residual stress in the welding process, resulting in the increase of hardness. The hardness of Samples 2, 4 and 6 is generally higher than that of Samples 1, 3 and 5, respectively, which indicates that the introduction of the additional shielding gas is beneficial for enhancing the hardness of the joint. The phenomenon may due to the introduction of additional shielding gas increasing the temperature gradient of the joints and accelerating the heat dissipation at the joints. With the increase in welding speed, the hardness of Samples 1, 3 and 5 increases gradually. Because the transformation time of ferrite decreases and austenite formation decreases with the increase in welding speed, relatively fine microstructures and increased hardness occur.

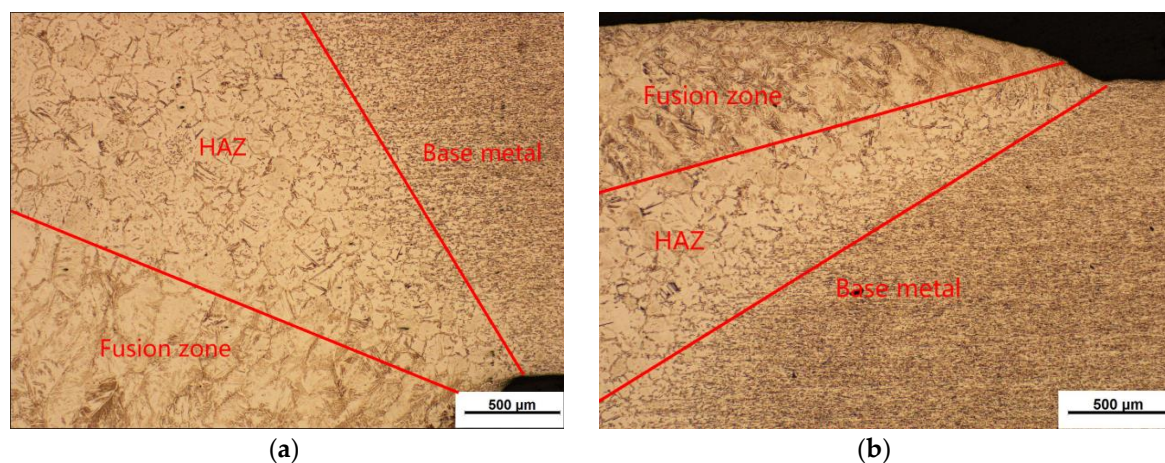


Figure 5. Cont.



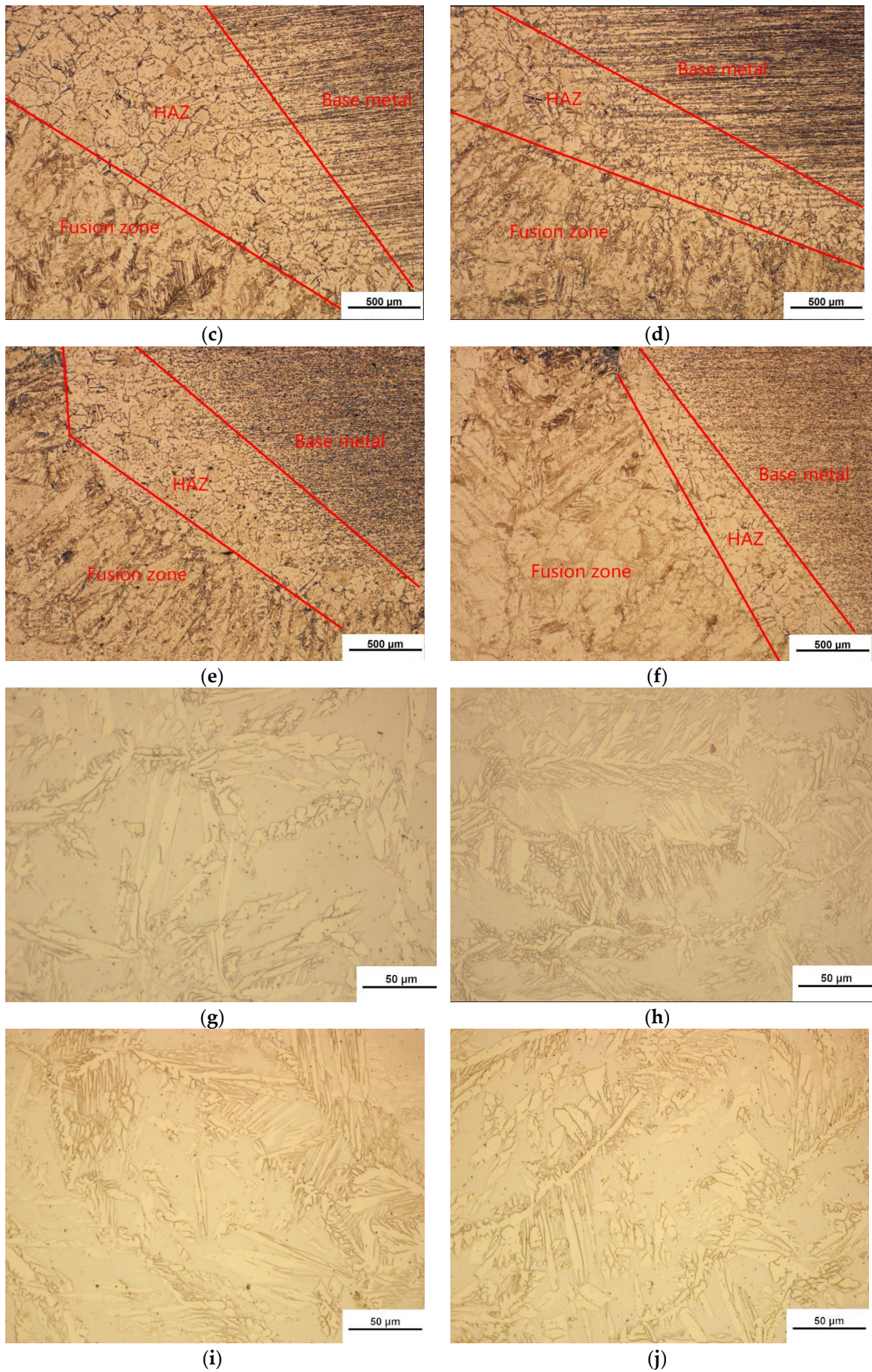
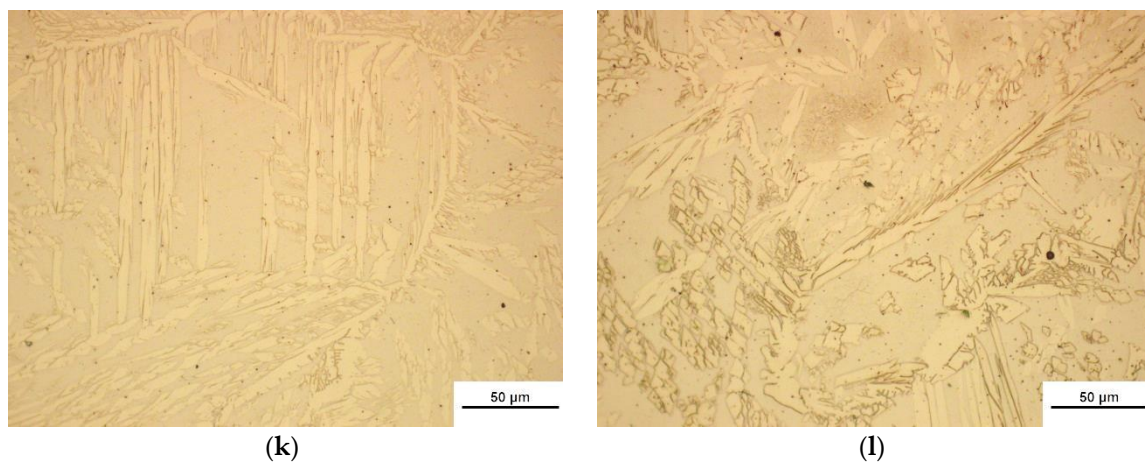
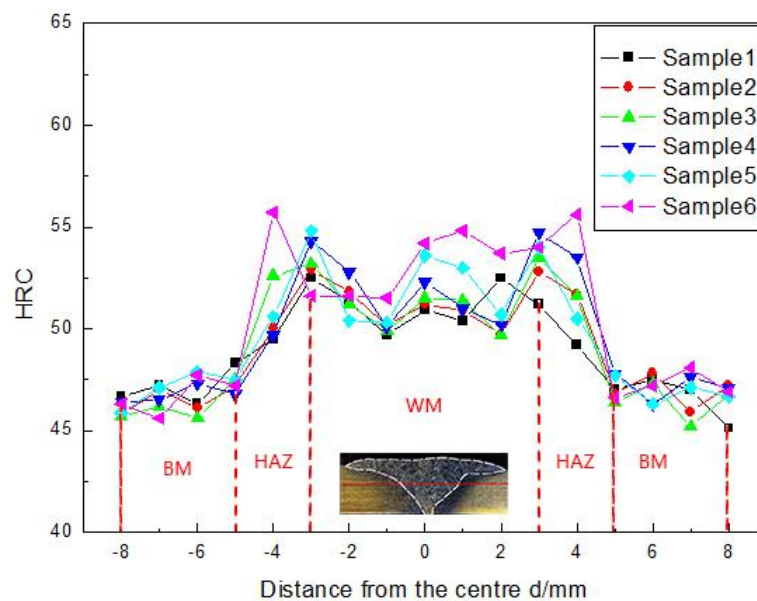


Figure 5. Cont.





**Figure 5.** Metallographic test results: (a) Metallographic image of HAZ in Sample 1, (b) Metallographic image of HAZ in Sample 2, (c) Metallographic image of HAZ in Sample 3, (d) Metallographic image of HAZ in Sample 4, (e) Metallographic image of HAZ in Sample 5, (f) Metallographic image of HAZ in Sample 6, (g) Metallographic image of fusion zone in Sample 1, (h) Metallographic image of fusion zone of in Sample 2, (i) Metallographic image of fusion zone in Sample 3, (j) Metallographic image of fusion zone in Sample 4, (k) Metallographic image of fusion zone in Sample 5, (l) Metallographic image of fusion zone in Sample 6.

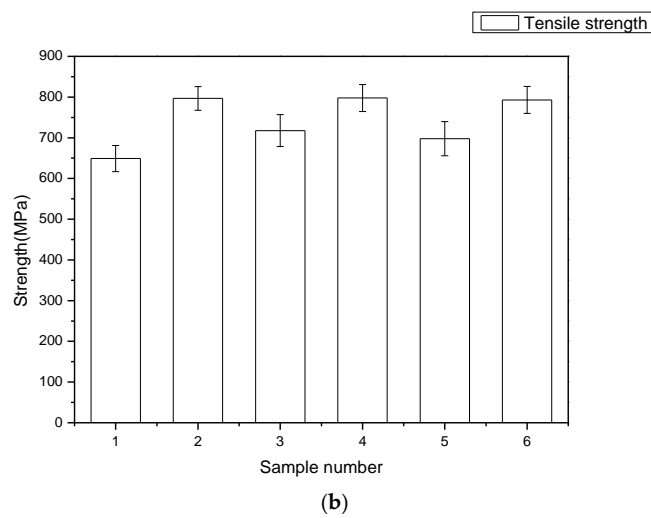
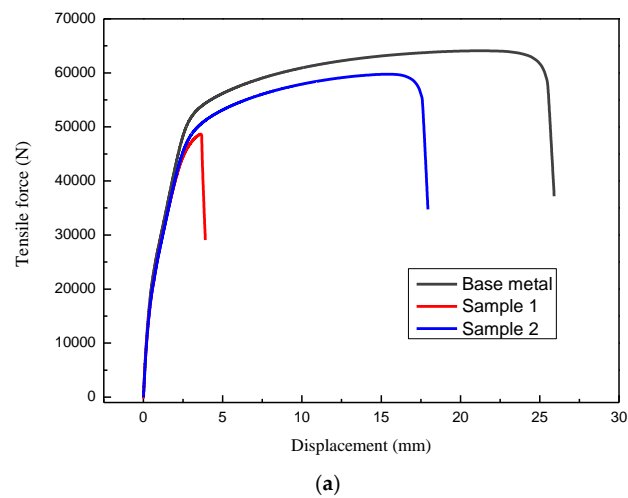


**Figure 6.** Rockwell hardness distribution in welded joints.

### 3.3. Mechanical Properties

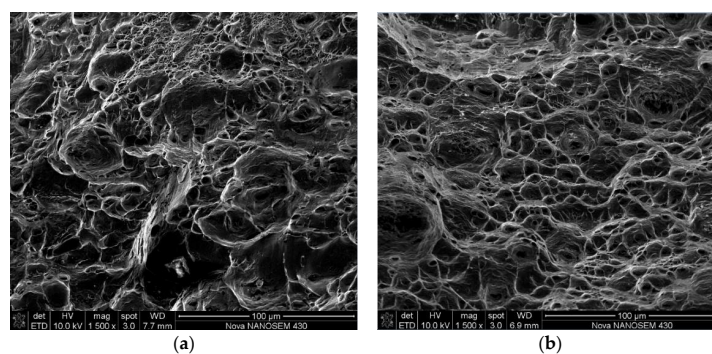
The tensile test results of the joints are shown in Figure 7. The tensile properties of the joints were significantly improved by introducing the additional shielding gas. The maximum tensile strengths of the samples 1–6 were 648 MPa, 776 MPa, 716 MPa, 775 MPa, 694 MPa and 773 MPa, respectively, which indicates that with the same welding current, the introduction of additional shielding gas increases the maximum tensile strength of the joint by 19.7%, 8.2% and 11.3% when the welding speed was 1.6, 1.8 and 2.0 m/min, respectively. The fracture cross-sections are shown in Figure 8. The fracture section of sample 1 shows a transgranular fracture along the cleavage plane because of the brittle fracture; the fracture section of Sample 2 shows a large number of irregular dimples, and the inclusion of second-phase particles can be observed at the bottom of the dimple, indicating that the joint fracture is ductile.





**Figure 7.** Tensile properties of the base metal and welded joint: (a) Tensile curves, (b) Result of tensile tests.

The Charpy impact test results of the joint and base metal are shown in Table 4. It can be seen from Table 4 that the average absorbed energy of the base metal is 54 J, while the average absorbed energy of the joints without the additional shielding gas ranges from 12 to 18.2 J, amounting to approximately 22.2–33.7% of the absorbed energy of the base metal. After introducing the shielding gas, the absorbed energy of the joints ranges from 27 to 30 J, amounting to approximately 50–55.6% of the absorbed energy of the base metal. At the same weld current and weld speed, the joint with additional shielding gas has a higher absorbed energy, and hence, better toughness.



**Figure 8.** Photographs of fractured tensile samples: (a) Sample 1, (b) Sample 2.

**Table 4.** Charpy impact test results of joint and base metal.

Sample Number	Absorbed Energy (J)				
	1	2	3	Average Value	Standard Deviation
Base Metal	53.5	53.8	54.7	54	0.5
1	17.9	18.1	18.6	18.2	0.3
2	29.7	30.1	29.6	29.8	0.2
3	11.8	11.8	12.4	12	0.3
4	30	29.9	30.1	30	0.1
5	17.5	17.3	16.8	17.2	0.3
6	26.8	26.9	27.3	27	0.2

#### 4. Conclusions

The introduction of additional shielding gas in twin wire double pulsed MIG high-speed welding can provide the following beneficial effects:

- (1) The welding process is more stable; the weld width is more uniform; the unfused defects of the weld can be effectively improved and diminished.
- (2) Due to the action of the external gas flow, the fluidity of the molten pool metal is better than that formed without additional shielding gas. The heat-affected zone is smaller than that of the weld seam formed without the additional shielding gas.
- (3) The tensile properties of the welded joints are significantly improved. When the welding speed was 1.6, 1.8, and 2.0 m/min, the maximum tensile strength of the joints increased by 19.7%, 8.2% and 11.3%, respectively.
- (4) At the same welding current and welding speed, the absorbed energy of the joint without the additional shielding gas ranges from 12 to 18.2 J (22.2–33.7% of the base metal), while the absorbed energy of the joint with the additional shielding gas ranges from 27 to 30 J (50–55.6% of the base metal), indicating that the joint with additional shielding gas has higher absorbed energy and better toughness.

**Author Contributions:** In this paper, J.X. gave guidance and advice about how to analyze the results of the research. Y.H. did the main writing of this paper. C.D., L.J. and Z.Z. provided considerable help with the experiment.

**Funding:** This research received funding from the National Natural Science Foundation of China (Grant No. 51875213), High-level Leading Talent Introduction Program of GDAS (Grant No. 2016GDASRC-0106), Natural Science Foundation of Guangdong (Grant No. 2016A030313117), Natural Science Foundation of Fujian (Grant No. 2018J01503), and Natural Science Foundation of Hainan (Grant No. 317288).

**Conflicts of Interest:** The authors declare no conflict of interest.

#### References

1. Chen, Y.; Liu, L.; Zhang, H. Effect of heat input on microstructure and toughness of weld joint of high strength low-alloy steel. *J. Shang Hai Jiao Tong Univ.* **2015**, *49*, 306–309.
2. Moinuddin, S.; Sharma, A. Arc stability and its impact on weld properties and microstructure in anti-phase synchronised synergic-pulsed twin-wire gas metal arc welding. *Mater. Des.* **2015**, *67*, 293–302. [[CrossRef](#)]
3. Gao, Y.; Huang, Z. Experimental analysis of weld formation in tandem twin-wire co-pool welding process. *Trans. China Weld. Inst.* **2016**, *37*, 21–24.
4. Wang, F.; Hua, X.; Ma, X.; Wu, Y.; Cao, N. Analysis of arc interference and interruption in double-wire GMAW welding. *Trans. China Weld. Inst.* **2011**, *32*, 109–112.
5. Ueyama, T.; Ohnawa, T.; Tanaka, M.; Nakata, K. Effects of torch configuration and welding current on weld bead formation in high speed tandem pulsed gas metal arc welding of steel sheets. *Sci. Technol. Weld. Join.* **2005**, *10*, 750–759. [[CrossRef](#)]
6. Ueyama, T.; Ohnawa, T.; Tanaka, M.; Nakata, K. Occurrence of arc interaction in tandem pulsed gas metal arc welding. *Sci. Technol. Weld. Join.* **2007**, *12*, 523–529. [[CrossRef](#)]

7. Ueyama, T.; Uezono, T.; Era, T.; Tanaka, M.; Nakata, K. Solution to problems of arc interruption and arc length control in tandem pulsed gas metal arc welding. *Sci. Technol. Weld. Join.* **2009**, *14*, 305–314. [[CrossRef](#)]
8. Sterjovski, Z.; Bayley, C.; Donato, J.; Lane, N.; Lang, D. Weld-End Solidification Cracking in Pulsed-Tandem Gas Metal Arc Welding of Naval Steels. *Weld. J.* **2014**, *93*, 145–152.
9. Wu, K.; Liang, Z.; He, Z.; Huang, X.; Cheng, J. Double-pulse multi-phase coordinative control system of high-power twin-wire GMAW. *J. South Chin. Univ. Technol.* **2016**, *44*, 40–45.
10. Gery, D.; Long, H.; Maropoulos, P. Effects of welding speed, energy input and heat source distribution on temperature variations in butt joint welding. *J. Mater. Process. Technol.* **2005**, *167*, 393–401. [[CrossRef](#)]
11. Armentani, E.; Esposito, R.; Sepe, R. The influence of thermal properties and preheating on residual stresses in welding. *Int. J. Comput. Mater. Sci. Surf. Eng.* **2007**, *1*, 146–162. [[CrossRef](#)]
12. Hazvinloo, H.; Honarbakhsh, A. Effect of gas-shielded flux cored arc welding parameters on weld width and tensile properties of weld metal in a low carbon steel. *J. Appl. Sci.* **2010**, *10*, 658–663.
13. Armentani, E.; Pozzi, A.; Sepe, R. Finite-element simulation of temperature fields and residual stresses in butt welded joints and comparison with experimental measurements. In Proceedings of the ASME 2014 12th Biennial Conference on Engineering Systems Design and Analysis, Copenhagen, Denmark, 25–27 July 2014.
14. Somashekara, M.; Naveenkumar, M.; Kumar, A.; Viswanath, C.; Simhambhatla, S. Investigations into effect of weld-deposition pattern on residual stress evolution for metallic additive manufacturing. *Int. J. Adv. Manuf. Technol.* **2017**, *90*, 2009–2025. [[CrossRef](#)]
15. Hang, Z.; Wu, D.; Zou, Y. Effect of bypass coupling on droplet transfer in twin-wire indirect arc welding. *J. Mater. Process. Technol.* **2018**, *262*, 123–130.
16. Wen, C.; Wang, Z.; Deng, X.; Wang, G.; Misra, R.D.K. Effect of heat input on the microstructure and mechanical properties of low alloy Ultra-High strength structural steel welded joint. *Steel Res. Int.* **2018**, *89*, 1700500. [[CrossRef](#)]
17. Ruan, Y.; Qiu, X.; Gong, W.; Wang, Y.; Sun, D. Effect of Cr<sub>2</sub>O<sub>3</sub> fluxes on the microstructures and penetration of twin wire MIG welded joint. *J. Jilin Univ.* **2012**, *42*, 651–655.
18. Cai, X.; Fan, C.; Lin, S.; Yang, C.; Hu, L.; Ji, X. Effects of shielding gas composition on arc behaviors and weld formation in narrow gap tandem GMAW. *Int. J. Adv. Manuf. Technol.* **2017**, *91*, 3449–3456. [[CrossRef](#)]
19. Reis, R.; Scotti, A.; Norrish, J.; Cuiuri, D. Investigation on welding arc interruptions in the presence of magnetic fields: Arc length, torch angle and current pulsing frequency influence. *IEEE Trans. Plasma Sci.* **2013**, *41*, 133–139. [[CrossRef](#)]
20. Ye, D.; Wu, D.; Hua, X.; Xu, C.; Wu, Y. Using the multi-wire GMAW processes for controlling the formation of humping. *Weld. World* **2017**, *61*, 649–658. [[CrossRef](#)]
21. Wu, D.; Hua, X.; Ye, D.; Ma, X.; Li, F. Understanding of the weld pool convection in twin-wire GMAW process. *Int. J. Adv. Manuf. Technol.* **2017**, *88*, 219–227. [[CrossRef](#)]
22. Wu, K.; He, Z.; Liang, Z.; Cheng, J. The dynamic behavior of double arc interference in high-power twin-wire pulsed GMAW. *Int. J. Adv. Manuf. Technol.* **2017**, *88*, 2795–2802. [[CrossRef](#)]

